International Journal of Heat and Mass Transfer 184 (2022) 122305

Contents lists available at ScienceDirect

International Journal of Heat and Mass Transfer

journal homepage: www.elsevier.com/locate/hmt

Deep learning techniques elucidate and modify the shape factor to extend the effective medium theory beyond its original formulation

Haofan Lu[a,1], Yi Yu[a,1], Ankit Jain[b], Yee Sin Ang[c], Wee-Liat Ong[a,d,e,*]

[a] ZJU-UIUC Institute, Zhejiang University, Haining, 314400, Zhejiang, China
[b] IIT Bombay, Powai, 400076, Mumbai, India
[c] Science, Mathematics and Technology, Singapore University of Technology and Design, Singapore, 487372, Singapore
[d] College of Energy Engineering, Zhejiang University, Hangzhou, 310027, Zhejiang, China
[e] State Key Laboratory of Clean Energy Utilization, Zhejiang University, Hangzhou, 310027, Zhejiang, China

ARTICLE INFO

Article history:
Received 26 August 2021
Revised 24 October 2021
Accepted 21 November 2021
Available online 3 December 2021

Keywords:
Multi-layer perceptron
Effective medium approximations
Machine learning
Neural network
Finite element

ABSTRACT

The effective medium theories (EMTs) can reliably approximate the property of a composite using properties of the inclusion and matrix phase. However, their inherent assumptions and the availability of mathematical forms for describing the inclusion structure limit their accuracy and applicability. In this work, we utilize the capabilities of a deep learning method to ameliorate the latter restriction for a particular EMT formulation. Our deep learning models elucidate the inclusion structure using several physics-based descriptors and can be easily adapted for other inclusion shapes through transfer learning. Using our models, we shed light on the interpretation of the shape factor in the chosen EMT. More importantly, we extend, not replace, the EMT for cases beyond its original formulation. Our proposed transfer learning approach requires relatively low computation cost and a small sample number, making it especially useful when new data is limited.

1. Introduction

The effective medium theory (EMT) is an analytical mean-field approach suitable for estimating various properties of a composite in many engineering and scientific fields [1–10]. In the thermal transport field, EMT is frequently employed as a first approximation to elucidate the thermal conductivity (K) results in experiments and simulations [11–18]. Its popularity over other methods (e.g., numerical simulations [19–21]) stems from its fast and reasonably accurate estimates while providing some physical insights. It also requires only relatively simple inputs like the thermal conductivity of the matrix (K_m) and inclusion (K_p) phases and volume fraction (f) of the inclusion phase. Its prediction accuracy, however, depends on its assumptions and the inclusion structures. Many of such EMTs are weighted combinations of five basic structural models [22,23]. Common in these models is a ubiquitous factor called the shape factor that accounts for the inclusion structure in the composite. For the same composite, this factor can have a different value in different EMTs and couples to K_m, K_p, and f in a complex and non-intuitive manner. Also, its physical interpretation is of ongoing scientific interest [22,23] and is suggested to be related to the number of Euclidean dimensions of the composite or the sphericity of the inclusion phase [24,25]. Advances in recent manufacturing technology can create many inclusions of complex shapes that enhance properties of a composite, including those for thermal transport [26–28]. Thus, an in-depth study of this factor will be beneficial for advancing the use of EMTs in meeting these new engineering demands.

Deep learning techniques have attracted recent interest for elucidating thermal transport problems at various length-scales [21,29–39]. The multilayer perceptron (MLP) model is one such deep learning technique that is inspired by the neural connections in a human brain [40–42]. The resulting network is used to classify new observations (i.e., as a classifier) or discover complex hidden input-output relationships for multi-variate predictions (i.e., as a regressor) and has been successfully employed in various thermal transport studies [32,33,43]. To date, most deep learning-based studies have focused on discovering intricate inputs-to-thermal-transport relationships using data collected from experiments and/or simulations. In this work, we utilize the deep learn-

* Corresponding author.
E-mail address: weeong@intl.zju.edu.cn (W.-L. Ong).
[1] Equal Contributions.

https://doi.org/10.1016/j.ijheatmasstransfer.2021.122305
0017-9310/

Nomenclature

K	effective thermal conductivity
Km	thermal conductivity of the matrix phase
Kp	thermal conductivity of the inclusion phase
f	volume fraction of the inclusion phase
p	aspect ratio
K_{FEM}	thermal conductivity computed by finite element
K_{EMT}	thermal conductivity computed by EMT
K_{MLP}	thermal conductivity computed by machine learning model
L_{ii}	geometrical factors dependent on the particle shape
a_i	length of axes of ellipsoid
V	volume
S	surface area
$FPro$	front projected area
$TPro$	top projected area
$RPro$	right projected area

ing techniques in another manner for another purpose. Instead of learning from experimental and simulation data to regress an input-output relationship, we employ the MLP model to investigate the physical meaning of the shape factor in an EMT and extend the EMT applicability beyond its original formulation. Our learning set, thus, comes from the analytical EMT equation, while our output is an improved EMT with broader applicability. The chosen EMT is a commonly used three-dimensional (3D) two-component equation that considers ellipsoidal inclusions. Such inclusions have a shape factor that is related to its mathematically definable aspect ratio, p [23]. We first train an MLP-based K-model with the K values calculated from this EMT equation. This approach allows us to obtain as much learning data as possible but with an accuracy limited by the EMT assumptions. Next, we introduce five physics-based shape descriptors to decompose and elucidate the shape factor by training another MLP-based p-model. Using this trained p-model, we extend the chosen EMT to calculate the K values for other inclusion shapes using transfer learning. The accuracy of these K predictions is evaluated against the solutions from a 3D heat diffusion equation solved using the finite element method. Our results suggest that we have successfully extended the original EMT to other inclusion shapes through transfer learning by modifying the shape factor. We also found that the ratio of the inclusion's projected areas is related to this shape factor.

The rest of this paper is organized as follows: Section 2 contains the descriptions of our methods and the tools used. Results from our deep learning models, the EMT, and the finite element models (FEMs) are compared and discussed in Section 3 before concluding in Section 4.

2. Methodology

The overall system architecture and investigation steps are shown in Fig. 1. Briefly, the selected analytical EMT formulation for ellipsoidal inclusions was used to generate the training and validation sets for the MLP-based K-model and p-model. The K-model uses input descriptors that are identical to the input parameters of the EMT. A well-trained K-model should, thus, predict a thermal conductivity value (i.e., K_{MLP}) similar to that of the EMT (i.e., K_{EMT}) for the same composite system. The p-model was trained using ellipsoidal inclusions to predict a p value for use in the EMT. The input descriptors for this model were derived from physics-based parameters that can influence heat transfer. This p-model was later used for transfer learning to generate p values for inclusion shapes with no analytical p. Data for transfer learning was generated using the FEM approach. With these p values, both the K_{EMT} and K_{MLP} were obtained and compared with the thermal conductivity results calculated from the FEM approach (i.e., K_{FEM}). Details of the individual steps are presented below.

We investigated the macroscopic thermal conductivity of 3D two-component composites with randomly oriented inclusions of identical shape and size. Here, the classical heat diffusion equation involving the Fourier law [44] can be solved without considering any size effects [20,31]. In addition, our study does not include cases where the interfacial thermal conductance between the matrix and inclusion phases is critical. The K of these 3D composites were obtained using three different approaches: 1) the EMT formulation (Eq. 1) [22,23] that was used to generate the training data for our MLP models, 2) our proposed MLP-based models (Fig. 2) for studying and extending that EMT and 3) a finite-element model that acted as the gold standard for comparison. The computational efficiency, model generalizability, and prediction accuracy for each of these approaches are briefly discussed in the Supplementary Material Section S1.

2.1. The EMT model

The chosen EMT formulation is originally derived by Nan et al. [23] for a composite containing randomly orientated ellipsoids. Here,

$$K = K_m \frac{3 + f[2\beta_{11}(1 - L_{11}) + \beta_{33}(1 - L_{33})]}{3 - f[2\beta_{11}L_{11} + \beta_{33}L_{33}]} \tag{1}$$

where K is the effective thermal conductivity. The shape factors L_{ii} are dependent on the inclusion shapes, with

$$L_{11} = L_{22} = \begin{cases} \frac{p^2}{2(p^2-1)} - \frac{p}{2(p^2-1)^{3/2}} \cosh^{-1} p, & for\ p > 1, \\ \frac{p^2}{2(p^2-1)} + \frac{p}{2(1-p^2)^{3/2}} \cos^{-1} p, & for\ p < 1, \end{cases}$$

$$L_{33} = 1 - 2L_{11}. \tag{2}$$

For an ellipsoid, $p = a_3/a_1$. Here, ellipsoids with two axes of equal length are used as the inclusion, i.e. $a_1 = a_2$ (see Fig. 1). β_{ii} are intermediate variables defined as:

$$\beta_{ii} = \frac{K_p - K_m}{K_m + L_{ii}(K_p - K_m)}, \tag{3}$$

As evident from the above three equations, p is related non-trivially to the shape factor. Eq. 1 was used to generate data for training and validating our K-model.

2.2. MLP-based machine learning model

We built two types of MLP models: 1) the K-model for learning the EMT formulation, and 2) the p-model to capture the relationship between our proposed shape descriptors and the effective p in Eq. 2. Their architectures are presented in Fig. 2. We used machine learning to learn the variable p instead of the variable L_{ii} in Eq. 2 as the former can be more easily generalized to other shapes and applied in other EMT formulations. The p-model is essential for understanding the physical meaning of the shape factor and extending the EMT to other shapes through transfer learning. Our MLP regressor was implemented using the scikit-learn library of Python [45]. The multiple layers of neurons in the MLP network were connected and activated by the non-linear ReLU function to enable non-linear regression [46,47]. Each connection was weighed by a parameter optimized by minimizing the mean square error

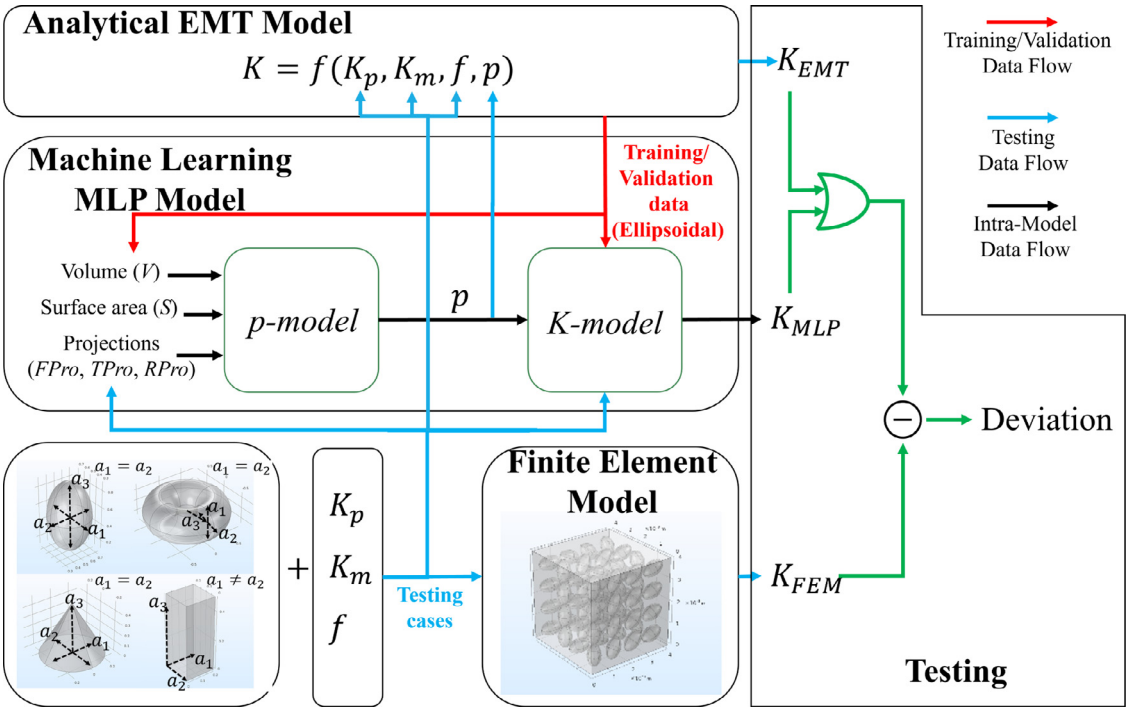

Fig. 1. The overall methodology and work flow.

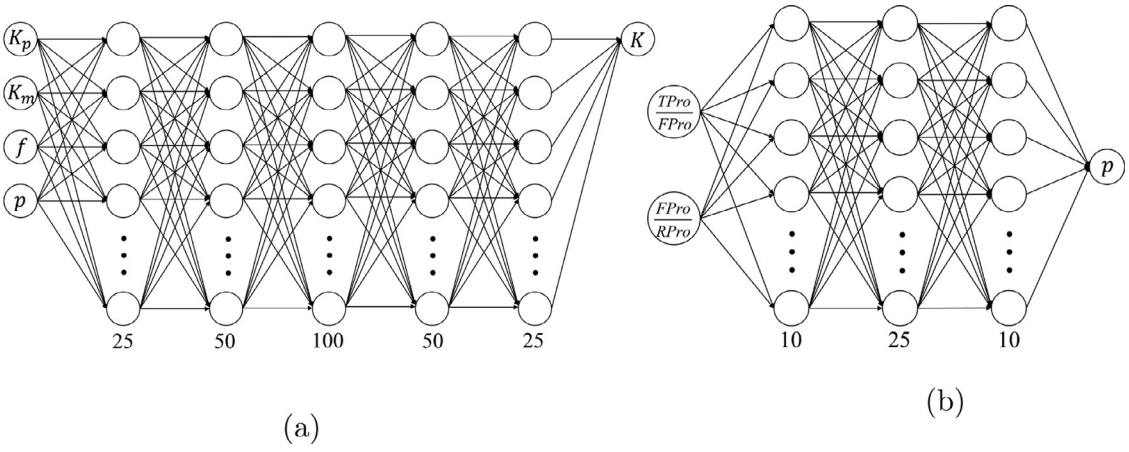

Fig. 2. The architectures of our MLP models: (a) *K*-model; (b) one of the three *p*-models. The other *p*-models are included in the Supplementary Material Section S2. The number below each hidden layer represents the number of neurons in that layer.

between the pairs of targeted and predicted values in the training set. Details for optimizing such MLP models can be found in ref. [33].

We quantified the results from our MLP-models using three evaluation metrics: a) the Pearson correlation coefficient, b) the root mean squared error (RMSE), and c) the relative root mean squared error (RRMSE). The Pearson correrlation coefficient measures the linear correlation between two variables and is bounded between −1 to 1. A value of 1 (-1) implies a perfect positive (negative) linear correlation between the variables, while a value of 0 indicates no linear correlation [48]. The RMSE, shown in Eq. 4, measures the quality of fit for a model. If the predictions ($pred_i$) are very close to the targets ($target_i$), the RMSE will be small. If some of the predictions and targets differ substantially, the RMSE might become large. A perfect fit between the predictions and targets will result in a zero RMSE. When an RMSE is normalized, the RRMSE is obtained. In this work, the mean value of the data set was used for normalizing. This metric allows for fair comparisons between data sets or models with different scales.

$$RMSE = \sqrt{\frac{1}{n}\sum_{i=1}^{n}(target_i - pred_i)^2} \tag{4}$$

2.2.1. The K-model trained to reproduce K values from the EMT

The *K*-model shown in Fig. 2a was trained using the *Adam* optimizer [49]. It has four input descriptors, five hidden layers, and one output node. Further details can be found in the Supplementary Material Section S2.

2.2.2. The p-model for capturing the inclusion's shape factor

The shape factor is ubiquitous in many different EMT formulations, indicating its importance for estimating *K*. Its physical interpretation, however, is an ongoing research question [22]. We attempt to shed light on this question by using several physics-based shape descriptors that can be obtained for most 3D inclusions. These descriptors were chosen based on the Occam's razor

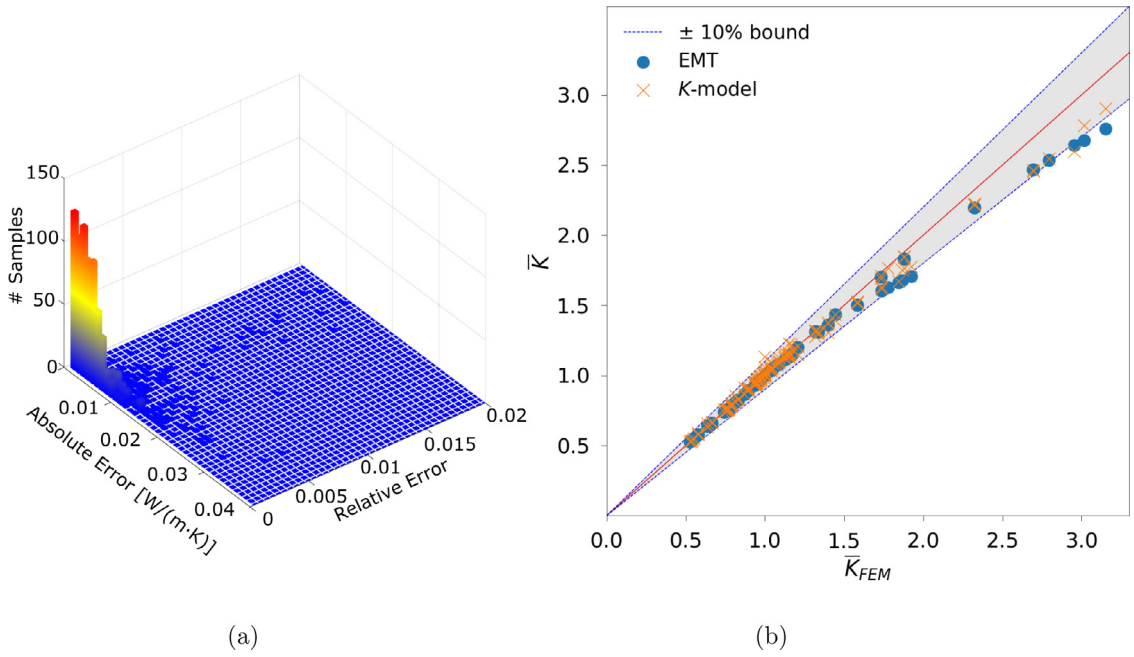

Fig. 3. (a) Histograms of the absolute and relative differences between the K predicted using the K-model and the EMT. (b) Comparison of the K predictions using the EMT and the K-model with the FEM results. An exact match between a K prediction and a FEM result will fall on the $y = x$ line in this figure. Note: K on both axes are normalized by the associated matrix phase thermal conductivity, i.e., $\overline{K} = K/K_m$ to amplify any small differences at small K_m values.

principle. We tested the simplest descriptors related to the heat transfer process first. These descriptors are the

1. volume of an inclusion (V),
2. surface area of an inclusion (S),
3. inclusion projected areas (*FPro*, *TPro*, and *RPro*)

An inclusion volume (V) contributes to its volume fraction in the composite. A larger inclusion volume fraction usually indicates a larger influence on the heat transfer process. A larger surface area (S) of an inclusion allows for more contacts between the inclusion and the surrounding matrix, increasing the heat transfer. This descriptor and V help to differentiate shapes with different surface-to-volume ratios. The projected areas (*FPro*, *TPro*, and *RPro*, see Fig. S6 of the Supplementary Material) are the cross-sectional areas perpendicular to the three principal heat flow directions, as defined in the 3D Fourier law. To avoid possible ambiguity arising from the positioning of an object, we assigned the biggest projected area as *FPro*, the second biggest one as *TPro*, and the remaining as *RPro*. Inclusions of different shapes and sizes were generated according to the orientations shown in Fig. 1 for training the p-model.

We investigated three different p-models to identify the critical descriptors for the shape factor. The architecture of one of the three p-models is shown in Fig. 2b. All p-models were first trained using ellipsoids and used for transfer learning to three other shapes (see insets in Fig. 1). For shapes that do not have mathematically definable p values (needed for transfer learning), we employed the maximum likelihood estimate approach to obtain them. Details for training the p-models and the subsequent transfer learning procedure are in the Supplementary Material Sections S2 and S3.

2.3. The FEM approach for thermal conductivity predictions

The FEM analysis is the gold standard for analyzing macroscopic thermal transport numerically [22]. Its drawback includes heavy computation resources and long computation time. Our FEM model is a $5 \times 5 \times 5$ cuboid with each unit cube containing a randomly oriented inclusion. Details of our FEM implementation are in the Supplementary Material Section S4.

3. Results and discussion

3.1. Comparison of K predictions with FEM results

The validation result for the K-model in Fig. 3a exhibits the characteristics of a well-trained model. 99% of the K_{MLP} have an absolute difference below 0.04 W/(m·K) while 97% are within a relative difference of 0.02 from the K_{EMT}. We also calculated the K_{FEM} of 147 different composites with randomly oriented ellipsoidal inclusions using the FEM approach. Fig. 3b shows that a majority of the K_{EMT} and K_{MLP} is within 10% of K_{FEM}. This close agreement suggests that the transport physics captured in the EMT equation is similar to that in the FEM approach.

3.2. Shape descriptors

As explained in Section 2.1, the shape factor of an ellipsoid is related to its analytically definable aspect ratio, p. As a first approach to elucidate the physical meaning of the shape factor, we calculated the Pearson correlation between p and our five shape descriptors proposed in Section 2.2.2.

These correlations were calculated using more than 900 randomly generated ellipsoids. The worst and best correlation result are shown in Figs. 4a and 4b. Correlation results for all five descriptors are included in the Supplementary Material Section S5 for completeness. As seen from these figures, none of these five simple descriptors correlates well with p. Instead of proposing new descriptors, we tested if combining some of these descriptors could improve the correlation score. Results from two such manual combinations are plotted in Figs. 4c and 4d. Given that two axes of our ellipsoids are identical and $p = a_3/a_1$, an appropriate ratio of the projected areas should show a strong correlation with p. As seen in Fig. 4(d), the correlation for the ratio *TPro*/*RPro* with p is strong

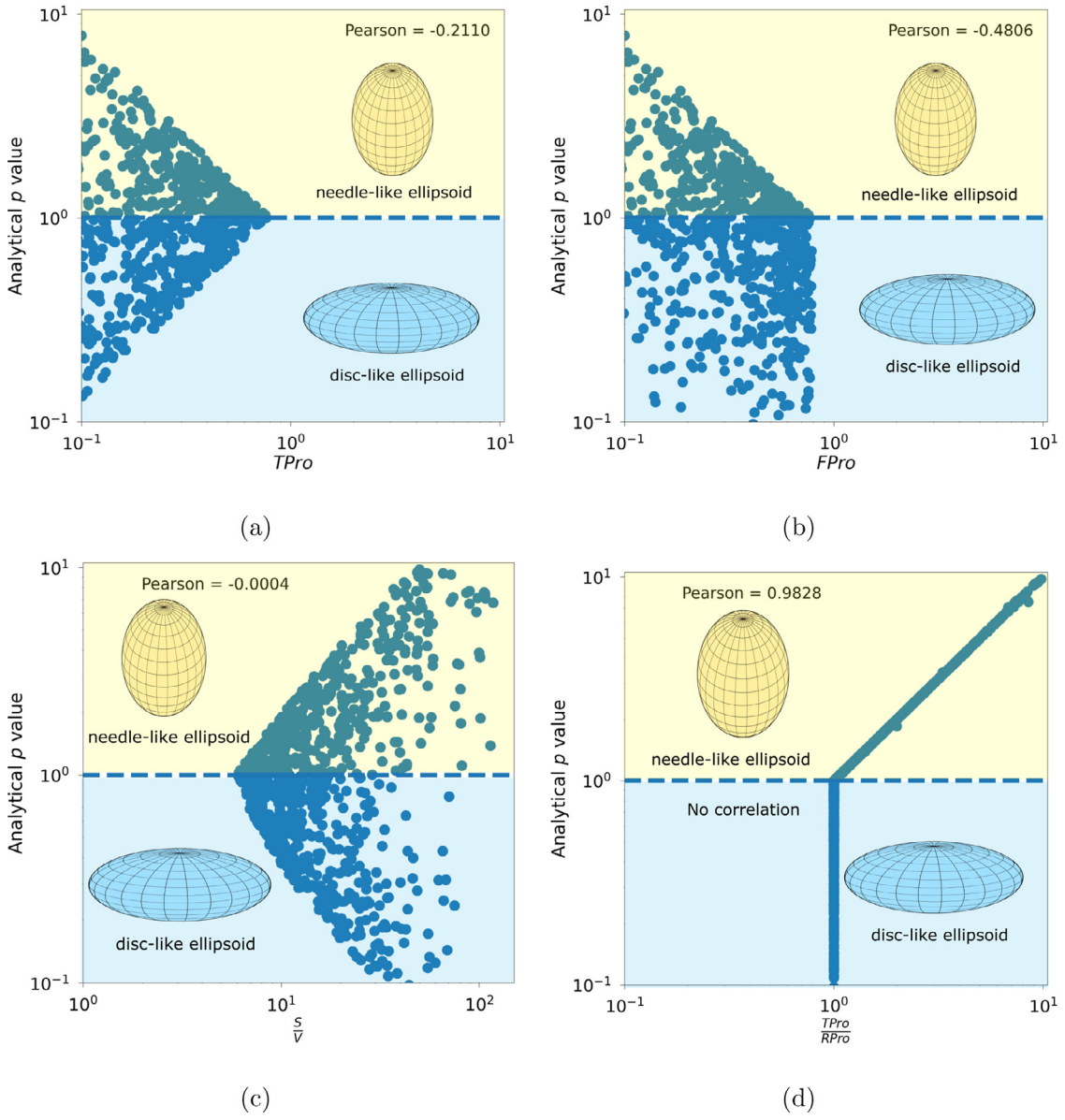

Fig. 4. The (a) worst and (b) best Pearson correlation with p for our five descriptors. (c) and (d) show the Pearson correlation from certain combinations of our descriptors.

when $p > 1$ but is undefined when $p < 1$. This behavior arises from how we defined our descriptors. Nevertheless, it is clear that certain combinations of our descriptors can better capture the characteristics of p. As manual testing requires a lot of time and effort, we built three MLP-based p-models to assist in discovering better correlations.

3.3. The shape factor model (p-model)

The three different p-models were trained with more than 900 thousand ellipsoids and validated with a separate set of one thousand ellipsoids. The descriptors for these p-models and their scores for the different evaluation metrics are tabulated in Table 1. The corresponding scores for the ratio $TPro/RPro$ are included for comparison. As seen from Table 1, the predictions from all three p-models exhibit excellent correlation with the analytical p, with low RMSE and RRMSE values. These values are also better than those obtained from the ratio $TPro/RPro$. An example of the correlation and the absolute difference is plotted in Fig. 5 using results from the 2-input p-model. Similar to the results in Table 1, Fig. 5a depicts an almost perfect Pearson correlation coefficient, indicating that our p-model can reliably estimate the analytical p value for $p > 1$ (needle-like) or $p < 1$ (disc-like). The absolute differences between its predictions and the analytical p values are less than 0.10 for 99% of the data (Fig. 5b).

Results from our p-models indicate that a combination of descriptors can have a high positive correlation with p even though the correlation of an individual descriptor is not high. Interestingly, the simplest 2-input p-model has the lowest RMSE value. It is more than five times smaller than those from the more complex 3-input and 5-input p-model. More descriptors, thus, may not be better and can degrade the performance. The ratios of the projected areas in the 2-input model are sufficient to fully capture the shape factor of an inclusion, alluding to the close relationship between these ratios and the shape factor. Nevertheless, the success of all three p-models allows us to decompose new shapes for extending the chosen EMT beyond its original formulation.

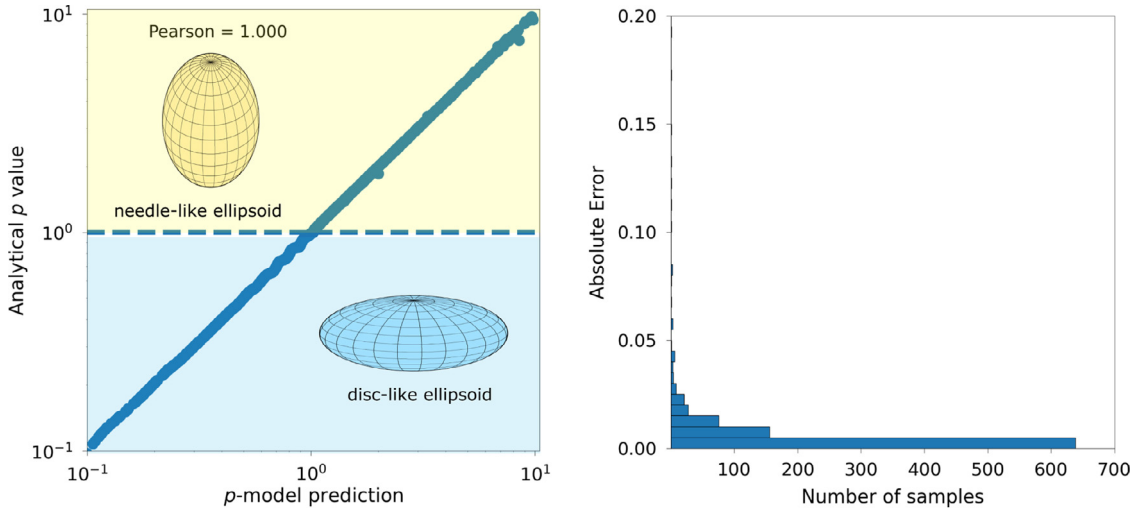

Fig. 5. (a) The p values of ellipsoids calculated from the analytical equation (Eq. 2) versus those predicted from the p-model. (b) The distribution of the absolute difference in the p values between the p-model and the analytical equation.

Table 1
Comparison of the various p-models.

Model Type	Descriptors	Pearson Correlation	RMSE	RRMSE
Ratio	*TPro/RPro*	0.983**	0.412	27.8%
2-input p-model	*TPro/FPro, FPro/RPro*	0.999	0.037	2.55%
3-input p-model	*FPro, TPro, RPro*	0.993	0.198	13.4%
5-input p-model	*S, V, FPro, TPro, RPro*	0.993	0.209	14.1%

**For $p > 1$.

3.4. Transfer learning to predict the p of other inclusion shapes and the K for such composites

Using our trained p-models, we extended the applicability of the EMT to composites with inclusions of unknown shape factors. The concept behind this is we approximated a new shape as an ellipsoid to obtain its effective p value for use in the EMT. Given that our p-models were trained using ellipsoids, they might not give the best p estimate for another shape. We, thus, exploited the MLP's adaptability for transfer learning to increase the accuracy of these p-models [50]. Transfer learning allows us to perturb and fine-tune these p-models using a relatively small number of samples. This property is advantageous for hard-to-obtain data and reduces computation time. As only a small number of data is needed, we used the more accurate FEM method to generate the required data for transfer learning. Composites with inclusions having the shape of a cone, torus, and cuboid were studied. Details of this transfer learning process are discussed in the Supplementary Material Section S3.

The p values for 40 independent samples of each new shape were predicted using the original and the transfer learning 2-input p-model. The corresponding K_{EMT} and K_{MLP} from these p values were calculated and compared to the K_{FEM} in Figs. 6a and 6b. Also included in these figures is the comparison of the K calculated using the ratio *TPro/RPro* with the K_{FEM}. In addition, we divided each figure into five equal sections along the x-axis and added the RRMSE of these three approaches in each section as bar charts. From these results, it is clear that these RRMSEs are quite low, with the lowest value coming from the transfer learning p approach. It is noteworthy that most of the predicted K are within 5% of the K_{FEM}, with the K_{EMT} being slightly more accurate than the K_{MLP}. This level of accuracy is as good as or better than most recent machine learning-based thermal conductivity studies that utilized EMT formulations [20,21].

Another interesting observation from Fig. 6 is that using the ratio *TPro/RPro* to calculate K_{EMT} for the new shapes can produce better results than using the original p-models. As p is not analytically defined for the other shapes, this result suggests that we can obtain good K_{EMT} estimates for other inclusion shapes by using *TPro/RPro* in place of the analytical p. Although we have performed further investigations (see Supplementary Material Section S6), the reason behind why *TPro/RPro* can produce good K estimates for other shapes is still an open question.

Fig. 6c depicts the overall RRMSE between the predicted K and the K_{FEM}. We have included the corresponding RRMSE of each p-model for the new shapes in the Supplementary Material Section S6. As mentioned above, the *TPro/RPro* can give more accurate K estimates than the original p-models. However, after transfer learning, the p-models yield better K_{EMT} values regardless of the inclusion shape. The overall RRMSE value is the lowest for the transfer learning 2-input p-model, highlighting the importance of the ratios of the projected area over the other descriptors.

Comparing the three subplots in Fig. 6, we see that the K-model has larger RRMSE values than the EMT. This result suggests that the K-model under-performs the EMT when predicting the K of composites with new inclusion shapes. Thus, in the presence of an analytical EMT equation, it is better to build a machine learning model for the critical unknown component (i.e., the p-model for the p values) to augment this equation for predicting K. A machine learning model for K itself is not essential. This result also potentially extends the original EMT formulation to shapes that can be mathematically difficult to describe while retaining the original insights from the EMT.

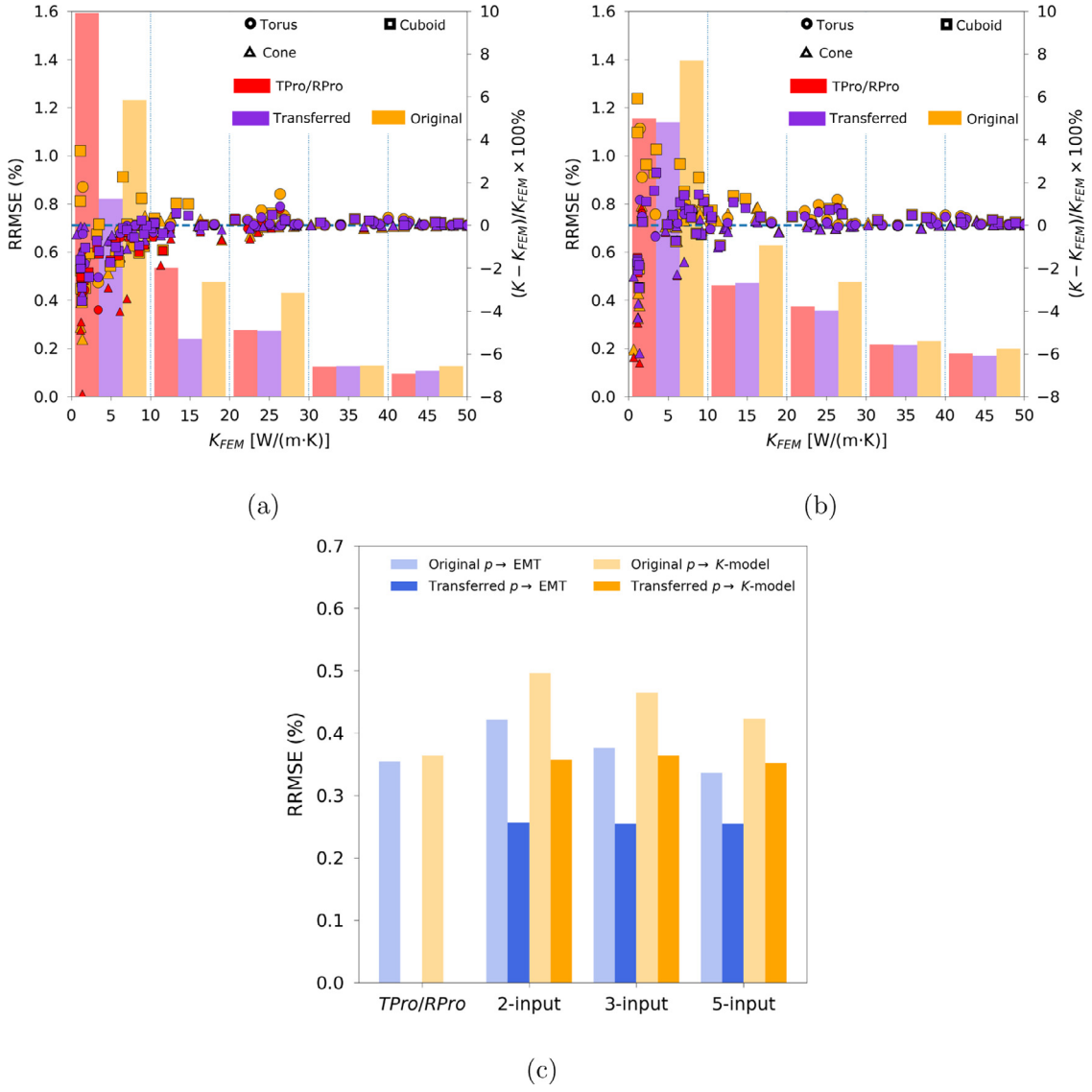

Fig. 6. Comparison of the K calculated using the a) EMT and b) K-model with K_{FEM} for composites with different inclusion shapes. The bar charts in each section of a) and b) represent the RRMSE between the K_{FEM} and K for the three approaches. The horizontal dotted line in both plots denotes the relative error at 0% while the vertical dotted lines demarcate each section that is used for the RRMSE calculation. c) The overall RRMSE of the K based on the different p approaches with K_{FEM}.

4. Conclusion

In this work, we present an MLP-based approach to extend a commonly used EMT formulation. To facilitate this goal, we build two types of MLP models (i.e., K-model and p-model) for this EMT. Our method conveniently allows us to generate large data sets for training. Our K-model can quickly estimate the thermal conductivity of composites with reasonable accuracy. As the K-model and the corresponding EMT formulation are restricted to its originally derived inclusion shapes, we devise three p-models to mitigate this restriction. In the process, we discover certain combinations of our proposed physics-based descriptors can better elucidate the effective p of any shapes. The predicted p value can be directly used in the EMT to obtain an accurate K estimate. Also, we demonstrate that the accuracy of our p-model for the new inclusion shape can be improved by a transfer learning process using a small number of samples (below 100). This process saves time and resources and can be particularly beneficial for hard-to-obtain data sets. Another interesting result from our work is that the ratio $TPro/RPro$ can replace the analytical p in the EMT to yield an accurate K_{EMT} for such composites. This result and those from the p-models suggest that the shape factor is related to the ratios of the projected areas in our chosen EMT. Our work presents a method to incorporate new complexities into classical physics-based equations using modern deep learning techniques. This procedure can be easily replicated to other fields with equations of a similar nature [8–10].

Declaration of Competing Interest

The authors declare that they have no known competing financial interests or personal relationships that could have appeared to influence the work reported in this paper.

CRediT authorship contribution statement

Haofan Lu: Methodology, Investigation, Writing – original draft. **Yi Yu:** Validation, Investigation, Writing – original draft. **Ankit Jain:** Writing – review & editing. **Yee Sin Ang:** Writing – review & editing. **Wee-Liat Ong:** Conceptualization, Supervision, Writing – original draft, Formal analysis, Writing – review & editing.

Acknowledgement

W.-L. Ong was the principal supervisor supported by the National Natural Science Foundation of China [grant number 51876186], Natural Science Foundation of Zhejiang Province [grant number LZ19E060002], and ZJU-UIUC Institute. Y. S. Ang and W-L. Ong acknowledge the support of IDEA SUTD-ZJU Visiting Professor Grant (Project No. ZJUVP2000101).

References

[1] Y. Li, X. Bai, T. Yang, H. Luo, C.-W. Qiu, Structured thermal surface for radiative camouflage, Nat. Commun. 9 (2018), doi:10.1038/s41467-017-02678-8.
[2] J. Li, Y. Li, W. Wang, L. Li, C.-W. Qiu, Effective medium theory for thermal scattering off rotating structures, Opt. Express 28 (18) (2020) 25894–25907, doi:10.1364/OE.399799.
[3] J. Li, Y. Li, T. Li, W. Wang, L. Li, C.-W. Qiu, Doublet thermal metadevice, Phys. Rev. Appl. 11 (2019) 044021, doi:10.1103/PhysRevApplied.11.044021.
[4] T. Koschny, M. Kafesaki, E.N. Economou, C.M. Soukoulis, Effective medium theory of left-handed materials, Phys. Rev. Lett. 93 (2004) 107402, doi:10.1103/PhysRevLett.93.107402.
[5] J. Huang, K. Yu, Enhanced nonlinear optical responses of materials: composite effects, Phys Rep 431 (3) (2006) 87–172, doi:10.1016/j.physrep.2006.05.004.
[6] S. Yang, J. Wang, G. Dai, F. Yang, J. Huang, Controlling macroscopic heat transfer with thermal metamaterials: theory, experiment and application, Phys Rep 908 (2021) 1–65, doi:10.1016/j.physrep.2020.12.006. Controlling macroscopic heat transfer with thermal metamaterials: Theory, experiment and application
[7] B. Tian, J. Wang, G. Dai, X. Ouyang, J. Huang, Thermal metadevices with geometrically anisotropic heterogeneous composites, Int J Heat Mass Transf 174 (2021) 121312, doi:10.1016/j.ijheatmasstransfer.2021.121312.
[8] S. Kirkpatrick, Classical transport in disordered media: scaling and effective-medium theories, Phys. Rev. Lett. 27 (1971) 1722–1725, doi:10.1103/PhysRevLett.27.1722.
[9] K. Busch, C.M. Soukoulis, Transport properties of random media: a new effective medium theory, Phys. Rev. Lett. 75 (1995) 3442–3445, doi:10.1103/PhysRevLett.75.3442.
[10] M. Zubair, Y.S. Ang, L.K. Ang, Fractional fowlernordheim law for field emission from rough surface with nonparabolic energy dispersion, IEEE Trans Electron Devices 65 (6) (2018) 2089–2095, doi:10.1109/TED.2017.2786020.
[11] W.-L. Ong, S.M. Rupich, D.V. Talapin, A.J.H. McGaughey, J.A. Malen, Surface chemistry mediates thermal transport in three-dimensional nanocrystal arrays, Nat. Mater. 12 (5) (2013) 410–415, doi:10.1038/nmat3596.
[12] H. Babaei, M.E. DeCoster, M. Jeong, Z.M. Hassan, T. Islamoglu, H. Baumgart, A.J.H. McGaughey, E. Redel, O.K. Farha, P.E. Hopkins, J.A. Malen, C.E. Wilmer, Observation of reduced thermal conductivity in a metal-organic framework due to the presence of adsorbates, Nat. Commun. 11 (1) (2020) 4010, doi:10.1038/s41467-020-17822-0.
[13] X. Hou, M. Wang, L. Fu, Y. Chen, N. Jiang, C.-T. Lin, Z. Wang, J. Yu, Boron nitride nanosheet nanofluids for enhanced thermal conductivity, Nanoscale 10 (2018) 13004–13010, doi:10.1039/C8NR00651B.
[14] M. Li, H. Zhou, Y. Zhang, Y. Liao, H. Zhou, Effect of defects on thermal conductivity of graphene/epoxy nanocomposites, Carbon N Y 130 (2018) 295–303, doi:10.1016/j.carbon.2017.12.110.
[15] G. Dai, J. Huang, Nonlinear thermal conductivity of periodic composites, Int. J. Heat Mass Transfer 147 (2020) 118917, doi:10.1016/j.ijheatmasstransfer.2019.118917.
[16] W.-L. Ong, S. Majumdar, J.A. Malen, A.J.H. McGaughey, Coupling of organic and inorganic vibrational states and their thermal transport in nanocrystal arrays, J. Phys. Chem. C 118 (14) (2014) 7288–7295, doi:10.1021/jp4120157.
[17] L.-W. Fan, X. Fang, X. Wang, Y. Zeng, Y.-Q. Xiao, Z.-T. Yu, X. Xu, Y.-C. Hu, K.-F. Cen, Effects of various carbon nanofillers on the thermal conductivity and energy storage properties of paraffin-based nanocomposite phase change materials, Appl Energy 110 (2013) 163–172, doi:10.1016/j.apenergy.2013.04.043.
[18] X. Fang, L.-W. Fan, Q. Ding, X. Wang, X.-L. Yao, J.-F. Hou, Z.-T. Yu, G.-H. Cheng, Y.-C. Hu, K.-F. Cen, Increased thermal conductivity of eicosane-based composite phase change materials in the presence of graphene nanoplatelets, Energy & Fuels 27 (7) (2013) 4041–4047, doi:10.1021/ef400702a.
[19] P. Jin, S. Yang, L. Xu, G. Dai, J. Huang, X. Ouyang, Particle swarm optimization for realizing bilayer thermal sensors with bulk isotropic materials, Int J Heat Mass Transf 172 (2021) 121177, doi:10.1016/j.ijheatmasstransfer.2021.121177.
[20] Z. Tong, M. Liu, H. Bao, A numerical investigation on the heat conduction in high filler loading particulate composites, Int. J. Heat Mass Transfer 100 (2016) 355–361, doi:10.1016/j.ijheatmasstransfer.2016.04.092.
[21] H. Wei, H. Bao, X. Ruan, Machine learning prediction of thermal transport in porous media with physics-based descriptors, Int. J. Heat Mass Transfer 160 (2020) 120176, doi:10.1016/j.ijheatmasstransfer.2020.120176.
[22] J. Wang, J.K. Carson, M.F. North, D.J. Cleland, A new approach to modelling the effective thermal conductivity of heterogeneous materials, Int. J. Heat Mass Transfer 49 (17) (2006) 3075–3083, doi:10.1016/j.ijheatmasstransfer.2006.02.007.
[23] C.-W. Nan, R. Birringer, D.R. Clarke, H. Gleiter, Effective thermal conductivity of particulate composites with interfacial thermal resistance, J. Appl. Phys. 81 (10) (1997) 6692–6699, doi:10.1063/1.365209.
[24] S. Kirkpatrick, Percolation and conduction, Rev. Mod. Phys. 45 (1973) 574–588, doi:10.1103/RevModPhys.45.574.
[25] H. Fricke, A mathematical treatment of the electric conductivity and capacity of disperse systems i. the electric conductivity of a suspension of homogeneous spheroids, Phys. Rev. 24 (1924) 575–587, doi:10.1103/PhysRev.24.575.
[26] X.-J. Wang, L.-Z. Zhang, L.-X. Pei, Thermal conductivity augmentation of composite polymer materials with artificially controlled filler shapes, J. Appl. Polym. Sci. 131 (8) (2014), doi:10.1002/app.39550.
[27] I.L. Ngo, V.A. Truong, An investigation on effective thermal conductivity of hybrid-filler polymer composites under effects of random particle distribution, particle size and thermal contact resistance, Int J Heat Mass Transf 144 (2019) 118605, doi:10.1016/j.ijheatmasstransfer.2019.118605.
[28] Y. Huang, C. Ellingford, C. Bowen, T. McNally, D. Wu, C. Wan, Tailoring the electrical and thermal conductivity of multi-component and multi-phase polymer composites, Int. Mater. Rev. 65 (3) (2020) 129–163, doi:10.1080/09506608.2019.1582180.
[29] H. Wei, H. Bao, X. Ruan, Genetic algorithm-driven discovery of unexpected thermal conductivity enhancement by disorder, Nano Energy 71 (2020) 104619, doi:10.1016/j.nanoen.2020.104619.
[30] P. Roy Chowdhury, C. Reynolds, A. Garrett, T. Feng, S.P. Adiga, X. Ruan, Machine learning maximized anderson localization of phonons in aperiodic superlattices, Nano Energy 69 (2020) 104428, doi:10.1016/j.nanoen.2019.104428.
[31] H. Wei, S. Zhao, Q. Rong, H. Bao, Predicting the effective thermal conductivities of composite materials and porous media by machine learning methods, Int. J. Heat Mass Transfer 127 (2018) 908–916, doi:10.1016/j.ijheatmasstransfer.2018.08.082.
[32] X. Wan, W. Feng, Y. Wang, H. Wang, X. Zhang, C. Deng, N. Yang, Materials discovery and properties prediction in thermal transport via materials informatics: a mini review, Nano Lett. 19 (6) (2019) 3387–3395, doi:10.1021/acs.nanolett.8b05196.
[33] A. Zendehboudi, R. Saidur, A reliable model to estimate the effective thermal conductivity of nanofluids, Heat Mass Transfer 55 (2019), doi:10.1007/s00231-018-2420-5.
[34] J. Carrete, W. Li, N. Mingo, S. Wang, S. Curtarolo, Finding unprecedentedly low-thermal-conductivity half-heusler semiconductors via high-throughput materials modeling, Phys. Rev. X 4 (2014) 011019, doi:10.1103/PhysRevX.4.011019.
[35] A. Seko, A. Togo, H. Hayashi, K. Tsuda, L. Chaput, I. Tanaka, Prediction of low-thermal-conductivity compounds with first-principles anharmonic lattice-dynamics calculations and bayesian optimization, Phys. Rev. Lett. 115 (2015) 205901, doi:10.1103/PhysRevLett.115.205901.
[36] S. Ju, T. Shiga, L. Feng, Z. Hou, K. Tsuda, J. Shiomi, Designing nanostructures for phonon transport via bayesian optimization, Phys. Rev. X 7 (2017) 021024, doi:10.1103/PhysRevX.7.021024.
[37] A. Jain, T. Bligaard, Atomic-position independent descriptor for machine learning of material properties, Phys. Rev. B 98 (2018) 214112, doi:10.1103/PhysRevB.98.214112.
[38] Y.-J. Wu, L. Fang, Y. Xu, Predicting interfacial thermal resistance by machine learning, npj Comput. Mater. 5 (1) (2019) 56, doi:10.1038/s41524-019-0193-0.
[39] B. Liu, L. Xu, J. Huang, Reinforcement learning approach to thermal transparency with particles in periodic lattices, J Appl Phys 130 (4) (2021) 045103, doi:10.1063/5.0054023.
[40] F. Rosenblatt, The perceptron: a probabilistic model for information storage and organization in the brain, Psychol Rev 65 6 (1958) 386–408.
[41] D.E. Rumelhart, G.E. Hinton, R.J. Williams, Learning Internal Representations by Error Propagation, MIT Press, Cambridge, MA, USA, p. 318362.
[42] K. Hornik, M. Stinchcombe, H. White, Multilayer feedforward networks are universal approximators, Neural Networks 2 (5) (1989) 359–366, doi:10.1016/0893-6080(89)90020-8.
[43] A. Najafi, M.E. Hamzehie, H. Najibi, M. Soleimani, T.V. Gerven, B.V.d. Bruggen, S. Mazinani, Thermal conductivity prediction of pure liquids using multi-layer perceptron neural network, J. Thermophys Heat Transfer 29 (1) (2015) 197–202, doi:10.2514/1.T4405.
[44] T. Bergman, A. Lavine, F. Incropera, D. DeWitt, Fundamentals of heat and mass transfer, Wiley, 2017.
[45] F. Pedregosa, G. Varoquaux, A. Gramfort, V. Michel, B. Thirion, O. Grisel, M. Blondel, P. Prettenhofer, R. Weiss, V. Dubourg, J. Vanderplas, A. Passos, D. Cournapeau, M. Brucher, M. Perrot, E. Duchesnay, Scikit-learn: machine learning in Python, J. Mach. Learn. Res. 12 (2011) 2825–2830.
[46] A.A. Minai, R.D. Williams, Original contribution: on the derivatives of the sigmoid, Neural Netw. 6 (6) (1993) 845853, doi:10.1016/S0893-6080(05)80129-7.
[47] V. Nair, G.E. Hinton, Rectified linear units improve restricted boltzmann machines, in: Proceedings of the 27th International Conference on International Conference on Machine Learning, in: ICML'10, Omnipress, Madison, WI, USA, 2010, p. 807814.
[48] A. King, R. Eckersley, Statistics for Biomedical Engineers and Scientists, Academic Press, London, 2019.
[49] D.P. Kingma, J. Ba, Adam: A method for stochastic optimization, in: Y. Bengio, Y. LeCun (Eds.), 3rd Int. Conf. on Learning Representations, ICLR 2015, San Diego, CA, USA, May 7–9, 2015, Conference Track Proceedings, 2015.
[50] S.J. Pan, Q. Yang, A survey on transfer learning, IEEE Trans. Knowl. Data Eng. 22 (10) (2010) 1345–1359, doi:10.1109/TKDE.2009.191.